Direct Numerical Simulation of Separated Turbulent Flow over a Wavy Boundary

Carsten Maaß and Ulrich Schumann

DLR, Institut für Physik der Atmosphäre
D-82230 Oberpfaffenhofen, Germany

Summary

The impact of a wavy surface on turbulent flow is investigated by direct numerical simulation. By means of finite differences in terrain following coordinates, the method treats the flow in a plane channel with wavy lower and flat top surfaces. Both surfaces are smooth. The lower surface wave amplitude is 0.05 and the wavelength is 1 in units of the mean channel height. The Reynolds number in terms of mean velocity and mean channel height is 6760. Parameter studies are performed with different resolution, Reynolds number and geometrical shape of the surface wave. If the vertical resolution is fine enough to resolve the viscous surface layer, a recirculation zone develops as expected for this surface geometry and Reynolds number. The comparison with existing experimental data shows good agreement when the precise details of the surface wave geometry, which deviates slightly from a sinusoidal profile, is taken into account.

Introduction

Turbulent boundary-layer flows in complex geometries are typical for environmental and technical flow problems. Traditional research on turbulent boundary layers considers flat plane channels and walls (Andrén et al. [2], Härtel and Kleiser [11], Schumann [24]) and pipes (Eggels et al. [9]). In this sense considering a plane channel with one wavy wall is a small step to more complex geometries. If one neglects friction and turbulence, i. e. considers a potential flow with constant mean streamwise velocity, the pressure variation at the surface is 180° out of phase with the wave and causes zero wave drag. Therefore disturbances decay exponentially with distance from the wall (Lamb [18]). Benjamin [3], using a curvilinear coordinate system, included friction and a mean boundary-layer velocity profile. He showed that the shear layer causes a phase shift of the velocity distribution that produces a drag. Thorsness et al. [26] found a quasi-laminar model sufficient to describe the wall shear stress for wavenumbers $2\pi\nu/(u_\tau\lambda) > 0.01$, but for smaller wavenumbers, the prediction of the phase shift is rather poor. Turbulence models using the van Driest function produce results which agree better with experiments (Kuzan et. al. [17]). For small amplitudes δ and large wavelength λ the flow responds linearly to sinusoidal disturbances. For large enough amplitudes the positive pressure gradient behind the wave is sufficient to cause separation. The flow over a train of waves differs from other separated flows [6] because the separation which may occur behind each wave crest affects the flow over the following waves.

All these models can describe some properties of the flow but no details of the separation. Recently, direct numerical simulations (DNS) of channel flow without separation above mild waviness were performed [12, 14], but in computational domains covering only one surface wave. Hino and Okumura [12] found stronger coherent eddy motion on the wavy wall than on the flat wall. The shear-stress distribution showed quasi-stationary streaky patterns corresponding to longitudinal vorticies. The waviness has little effect on the total bottom drag. Simulations of flows over two- and three-dimensional rough hills have been made by Wood and Mason [28] using a numerical model which employs a $1\frac{1}{2}$-order turbulence closure model.

Zilker and Hanratty [30] gave an overview on experimental work, from which the bulk of our understanding of such flows is mainly derived. The experiments concentrated on the measurement of surface pressure, wall shear stress, and velocity components. Motzfeld [21] pointed to the difference between roughness and waviness. Zilker et al. [29] showed that the wall shear stress is a better measure for the linearity of the flow than the velocity.

Buckles et al. [5] found a thin turbulent boundary layer which forms behind the reattachment point and extends to the next separation point. There, a free shear layer develops away from the wall behind the next reattachment point, so that there are now two layers above each other. Gong et al. [10] examined a flow above a wavy wall at two different surface roughnesses. The measurements exhibited an approximately two-dimensional flow with separation over the relatively rough surface. Over the smoother surface they observed a three dimensional secondary flow. The findings can be well modeled by large-eddy simulations (LES). The experiments of Kuzan et al. [17] with $\delta/\lambda = 0.1$ show a decreasing separation with increasing Reynolds number.

Recently, Hudson [13] made measurements in a water channel for two different amplitudes and several flow rates. For a case with separation in the mean flow field, he investigated how the Reynolds stresses and turbulence production differ from what would be observed over a flat wall.

Most theoretical studies were two-dimensional and limited to cases with weak nonlinear effects. Experiments were carried out for a wide set of parameters but not directly comparable and sufficient for turbulence modelling. There is little information about the three-dimensional structures. Considering turbulent separated flow over a wavy wall [1] as a test case for advanced statistical turbulence models, it has been shown recently that these models are still not able to really predict the flow [22]. There is a need for well defined experiments as well as for results from direct numerical simulations. The data presented here could be helpful for improving statistical models as well as LES models, e. g. Breuer and Rodi [4].

In a previous article [20], results of DNS at $Re = 4780$ have been shown and compared to experimental data. There we did not reach complete agreement with the laboratory measurements. In the mean time it turned out that the Reynolds number in the experiment was 6760 instead of 4780 as reported initially. Also the shape of the surface wave differed slightly from the purely sinusoidal shape assumed before. In this study we investigate the three-dimensional nonlinear flow at $Re = 6760$ over a wave which approximates the measured surface shape by means of DNS and compare the results to revised experimental data of Hudson [13].

Method

The method is explained in detail by Krettenauer and Schumann [16]. In this study the model uses grid refinement near the walls, contains different boundary conditions, and is applied to a flow with higher requirements on the accuracy of the method because of thinner shear layers at the surface. For these reasons it still remains to validate the code although the present numerical method has been used for DNS and LES of turbulent convection over wavy boundaries without [16, 23] and with mean flow [7, 8, 19].

The basic equations describe the conservation of mass and momentum for incompressible flows,

$$\frac{\partial u_j}{\partial x_j} = 0, \tag{1}$$

and

$$\frac{\partial u_i}{\partial t} + \frac{\partial}{\partial x_j}(u_j u_i) = -\frac{\partial p}{\partial x_i} + \frac{1}{Re}\frac{\partial^2 u_i}{\partial x_j{}^2} + P_x \delta_{1i}, \qquad i = 1,2,3, \tag{2}$$

where u_i denotes the velocity components, x_i the Cartesian coordinates, t the time, p the deviation from a reference pressure p_0, P_x the driving pressure gradient in x-direction and $Re = UH/\nu$ the Reynolds number for unit density. All quantities are made dimensionless with the channel height H, with the mean streamwise velocity U, with the time scale $t/t_{\mathrm{ref}} = H/U$ and density $\rho = \mathrm{const}$. The equations of motion are formulated for the Cartesian velocity components (u, v, w) as a function of curvilinear coordinates $(\overline{x}, \overline{y}, \overline{z})$ which are related to the Cartesian coordinates according to the transformation $\overline{x} = x$, $\overline{y} = y$, $\overline{z} = \eta(x, y, z)$. Here,

$$\eta = H\frac{z-h}{H-h} \tag{3}$$

maps the domain above the wavy surface at height $h(x, y) = \delta\cos(2\pi x/\lambda)$ and below a plane top surface at $z = H$ onto a rectangular transformed domain. The geometrical parameters are H, the lateral lengths L_x and L_y, the wave amplitude δ, and the wavelength λ, see Figure 1. To get higher resolution at the rigid top and bottom surfaces we use an additional hyperbolical transformation function of a coordinate ξ which is discretized equidistantly,

$$\eta = \frac{H}{2}\left(1 + \frac{\tanh(c_g\,\xi)}{\tanh c_g}\right), \quad -1 \le \xi \le 1. \tag{4}$$

The parameter c_g is choosen so that two adjacent grid spacings $\Delta\eta$ differ by less than 11 %.

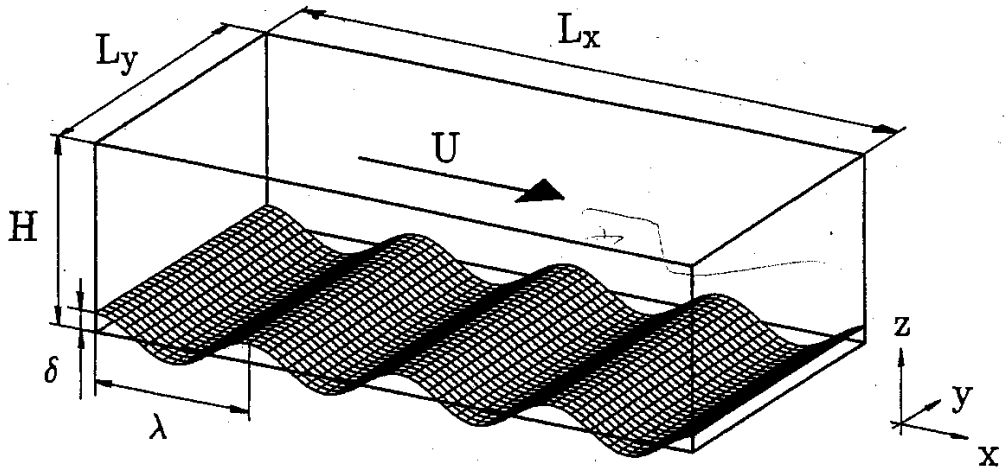

Figure 1: Perspective view of the computational domain in three dimensions showing the sinusoidal surface-wave in x-direction; the surface height is constant in y-direction. In this example, the wavelength is $\lambda = 1$, the wave-amplitude is $\delta = 0.1$, and the domain-size is $H = 1$, $L_x = 4$, and $L_y = 2$.

The differential equations are approximated by finite differences in a spatial staggered grid. The first discrete grid point for the horizontal velocity components is located $\Delta\eta/2$ above the wall. The momentum equation is integrated in time using the Adams-Bashforth scheme. The mean velocity U is defined as the average velocity in the x-direction across a y-z plane at a position with vanishing wave amplitude. After each time step Δt, the actual mean velocity is tested and a mean pressure gradient P_x in the axial direction is determined such that U remains constant. The pressure is determined iteratively. After five iterations the divergence in the first grid level above the bottom surface is reduced to $10^{-3}U/H$. At other grid levels it is lower by the order of 3 magnitudes. Periodicity conditions are used at the lateral boundaries. At the bottom and top surfaces we implement the no-slip condition.

The initial conditions prescribe uniform velocity at every grid point. Random perturbations are added to the velocity field which eventually becomes turbulent. This situation is comparable to turning on the pump in a laboratory set-up. The details of this initialisation are unimportant for the final statistics at late times of the simulation.

The simulations are performed on the DLR high performance computers Cray-YMP and NEC SX-3. All cases are at least run until the final dimensionless time $t_{\text{ref}} = H/U = 70$, which required 15 h CPU time on the NEC SX-3 using $256 \cdot 128 \cdot 96$ grid points. The obtained perfomance on the NEC SX-3 is 20% of the peak performance and at least 7 times higher as on the Cray-YMP. The internal data management, which is carried along although it is not needed, devides the data in vertical x-z slices. This embarrasses optimal vectorisation for the used number of grid points. For the future, we plan to parallelize the code by using parallel algorithms as described in Schumann and Strietzel [25].

Results and Discussion

We report below results obtained from a set of direct numerical simulations with different Reynolds numbers, bottom shapes, and resolutions, see Table 1, which were performed during the approach to an experimental set-up. In all cases the longitudinal domain size extends over 4 surface wavelengths. The lateral domain size should be large enough to cover the largest turbulent structures. The wave amplitude $2\,\delta/\lambda$ is 0.1 in all cases. The horizontal grid spacings are equal ($\Delta x = \Delta y$). The Reynolds number in DNS 5 (see [20]) is smaller by a factor of $\sqrt{2}$ than in all other cases. The parameters of DNS 1, which corresponds to our best knowledge to the experiment wb3 in the thesis of Hudson [13], differ from DNS 2 only in the shape of the wavy bottom (see below). DNS 2 to 4 differ only in resolution. DNS 4 is the only run with equidistant vertical grid spacing. All other cases use variable grid spacings with maximum resolution near the top and bottom surfaces. Using the friction velocity at the wavy bottom $u_{\tau,\mathrm{wa}}$, the finest resolution in terms of viscous scale is $(\Delta x^+, \Delta \eta^+) = (10.2, 1.6)$ for case 1. This is still at the limit of what is required to resolve the viscous sublayer, but of the same order as in other successfull DNS calculations [15, 27].

From the map of Zilker and Hanratty [30] one expects turbulent flow with mean separation for all cases in Table 1.

Table 1: Model parameters of various DNS. In all cases the computational domain extends over $4\,H \times 2\,H \times 1\,H$; $\Delta x^+ = \Delta y^+$ denotes the horizontal mesh size, $\Delta \eta^+$ the mesh height, c_g the parameter in equation (4), $\Delta(\Delta\eta) = (\frac{\Delta\eta_{k+1}-\Delta\eta_k}{\Delta\eta_k})_{\max}$ the difference between two adjacent grid spacings, Δt the nondimensional time step, $u_{\tau,\mathrm{fl}}$ and $u_{\tau,\mathrm{wa}}$ the nondimensional friction velocity at the flat and wavy wall, respectively. Values marked with $^+$ are made nondimensional with wall units. DNS 1 is performed with the experimental wave profile, all other simulations with a sinusoidal bottom.

DNS	Re	$N_x \cdot N_y \cdot N_z$	c_g	Δt	Δx^+	$\Delta(\Delta\eta)$	$\Delta\eta^+_{\min}$	$\Delta\eta^+_{\max}$	$u_{\tau,\mathrm{fl}}$	$u_{\tau,\mathrm{wa}}$
1	6760	$256 \cdot 128 \cdot 96$	1.7	0.003	10.2	0.068	1.6	12.4	0.070	0.097
2	6760	$256 \cdot 128 \cdot 96$	1.7	0.003	10.9	0.068	1.8	13.3	0.070	0.104
3	6760	$96 \cdot 48 \cdot 48$	1.4	0.009	30.1	0.107	5.4	23.8	0.071	0.107
4	6760	$80 \cdot 40 \cdot 40$	1.0	0.010	33.8	0.000	16.9	16.9	0.074	0.100
5	4780	$160 \cdot 80 \cdot 64$	1.4	0.006	12.4	0.079	2.7	12.2	0.071	0.104

By monitoring the kinetic energy E_{kin} of the whole domain we made sure that the flow is sufficiently stationary at the end of the simulation (Figure 2). The evolution of E_{kin} for DNS 1 – 3 is very similar and distinct from DNS 4, the only case without separated region. It can be seen already from this picture, that the mean separated flow is not influenced very much by resolution and by details of the surface wave. Due to the random perturbations, adjustment to the boundary conditions, and realisation of the continuity equation, all curves start slightly above the theoretical value of 0.5. Before $t/t_{\mathrm{ref}} = 5$ a relative maximum is passed which is caused by the growth of initial vorticies in the trough

region. From studying instantaneous flow fields at early times of the simulations, we know that first one almost laminar vortex in spanwise direction appears at the downslope side of the wave. While this vortex moves in upstream direction through the trough region it gets stronger and forces the mean flow towards the center of the channel. After that, more but weaker vorticies appear at the downslope side of the wave while the primary vortex disappears under the action of strong shear at the upslope side of the wave. Finally a relatively small separated region remains which is nearly unchanged for $t/t_{ref} > 4.5$. The following time evolution is mainly caused by processes connected with the development of shear layers near the walls, as in a flat channel. For the coarsest grid and for equidistant vertical resolution (DNS 4) the results do not show a separation. The separation arises only in a transient initial phase but disappears at later times. For all DNS it takes about $50\,t/t_{ref}$ to reach stationarity. For statistical evaluation the three-dimensional flow fields are averaged over the last $10\,t/t_{ref}$ with an interval of $0.5\,t/t_{ref}$.

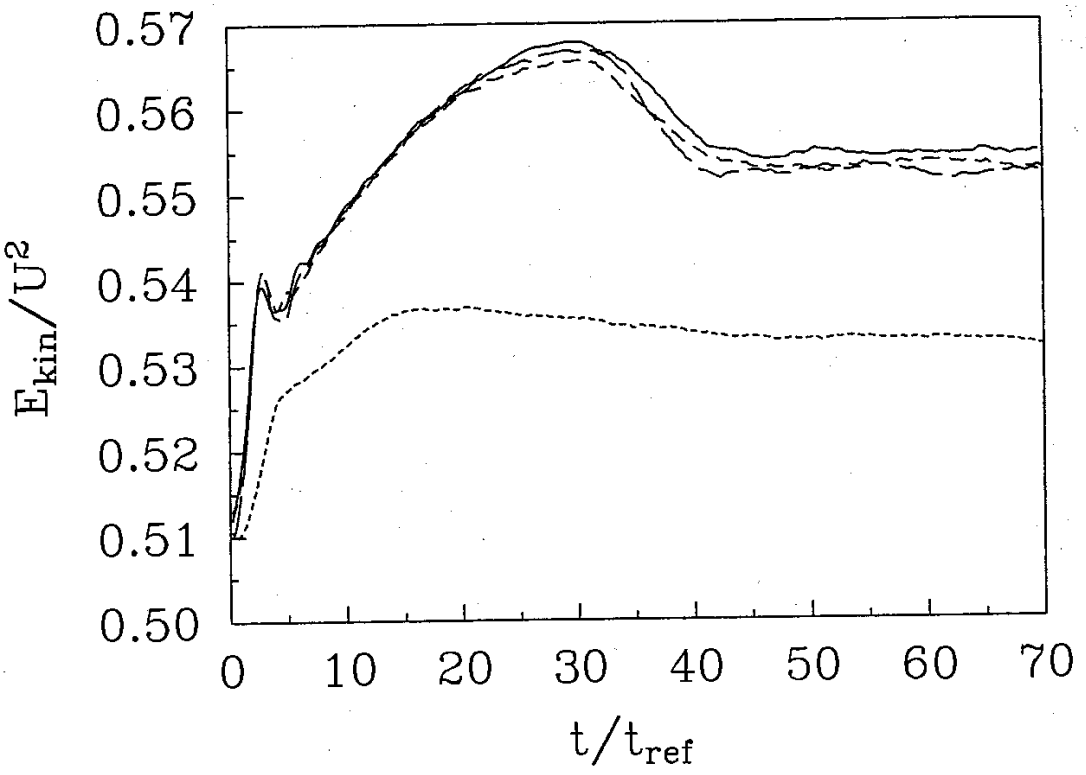

Figure 2: Volume averaged kinetic energy E_{kin} versus time t. —— DNS 1, — — DNS 2, - - - DNS 3, - - - - - DNS 4.

Of main interest for applications is the vertical flux of downstream momentum τ. It is composed of advective contributions due to the mean flow field and frictional parts due to turbulent fluctuations. Both contributions are modified by the wavy wall. In addition, at wavy surfaces the pressure causes a further contribution $\tau_{pres} = \overline{p(\partial z/\partial x)_\eta}$, where the bar denotes the horizontal average over coordinate planes η = const. The pressure

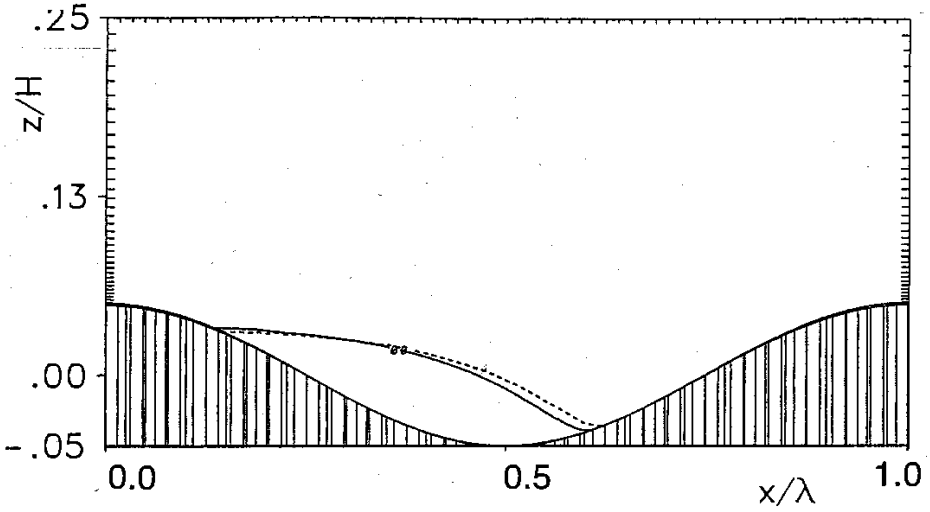

Figure 3: Mean streamline $\Phi = 0$ of DNS 2 (—) and DNS 5 (– – –).

contribution is strongly influenced by the shape of the bottom surface and of the separated region. Because it exceeds the sum of advectional and frictional momentum transport it is mainly responsible for the total drag at the lower boundary. The friction velocities in Table 1 are computed from the sum of the three contributions to the momentum flux.

The friction velocity at the flat wall varies only by about 1.5% for all cases with recirculation, so the influence of resolution, Reynolds number, and bottom surface on the upper boundary is very small. On the contrary, comparing the friction velocity at the lower boundary from DNS 1 and 3 we find a difference of about 10%. Comparing DNS 1 and 2 the difference of about 7% is due to the small differences in the shape of the bottom surface. This shows for the considered flows, that the shape of the surface wave has relatively large influence. Mainly because of the additional pressure forces, the effective friction velocity is up to 50% (DNS 3) larger at the wavy surface than at the flat surface.

Hino & Okumura [12] found for flow without recirculation that the total shear stress on the upper flat wall decreases a little compared with that over the flat parallel bottom. In all of our simulations the total shear stress at the flat wall is significantly higher as proposed e.g. from Blasius' law.

The mean streamline $\Phi = 0$ bounds the separated region. In Figure 3 the separated region is shown for two simulations with different Reynolds numbers. For $Re = 6760$ and 4780 the influence of Reynolds number is small. Corresponding to other observations [17] the size of the separated region decreases slightly with increasing Reynolds number.

As already shown for the lower Reynolds number [20], the flow structure near the wavy surface shows a streaky pattern with downstream elongated vortices at the upstream slope but less regular patterns on the downstream side. The spanwise spacing of the regular patterns is about $0.3\,H$.

Now we compare the results of DNS 1 with experimental data from Hudson [13]. The parameters of the DNS correspond to a water channel with channel height $H = 50.8$ mm,

Table 2: Profile of Hudson's wave. Accuracy of locating surface height h: $0.2 \cdot 10^{-3} H$.

x/λ	0.0	0.1	0.2	0.3	0.4	0.5	0.6	0.7	0.8	0.9
h/H	0.1	0.089	0.066	0.036	0.0095	0.0015	0.0195	0.0505	0.0785	0.095

Table 3: Fourier coefficients a_l and b_l of the harmonic analysis of Hudson's wave model.

Mode l	a_l	b_l	$\sum \delta^2$
0	$.109E+00$	$.000E+00$	$.418E-01$
1	$.484E-01$	$-.702E-02$	$.846E-04$
2	$-.391E-02$	$.996E-03$	$.312E-05$
3	$.736E-03$	$.131E-03$	$.329E-06$

wave amplitude $2\,\delta/\lambda = 5.08$ mm, wave length $\lambda = H$, the mean velocity $U = 122.2$ mm/s, and $Re = UH/\nu = 6760$. In the simulation we used the Fourier series

$$z_s/H = \sum_{l=1}^{3} \left(a_l \cos\left(2\pi \frac{lx}{\lambda}\right) + b_l \sin\left(2\pi \frac{lx}{\lambda}\right) \right), \tag{5}$$

with the coefficients shown in Table 3 to represent the experimental bottom surface from Table 2. Note that in equation (5) $a_0/2$ is neglegted in order to obtain vanishing mean wave height. This curve mainly differs at the upslope side from the ideal cosine profile with wave amplitude $\delta = 0.05\,H$ and wavelength $\lambda = 1\,H$ which has been used for the other simulations. To our best knowledge the only difference to Hudson's case wb3 concerns the mean velocity. In the simulation we used the mean over the whole channel U to build the Reynolds number while Hudson used the mean velocity U_{ref}, which is an average solely in the lower half of the channel. Because of the asymmetric mean profile U_{ref} is smaller than the bulk velocity U of the whole channel. For DNS 1 we get $U_{\text{ref}} = 0.912\,U$, so the Reynolds number may be in effect about 9 % smaller in the computation than in the experiment. For the purpose of comparing simulation and experiment, the velocities are made dimensionless with U_{ref}. From the picture in Figure 3 we assume that the influence from changing the Reynolds number by 10% should be negligible.

Figure 4 depicts profiles of the computed and measured velocities and turbulence quantities. The numerical results are ytp-mean values, i. e. averages over the y coordinate, time ($60 < t/t_{\text{ref}} \leq 70$), and over the four surface positions of equal phase angle. The streamwise velocity profiles (Figure 4 a) are characterised by very strong vertical gradients at the upslope side of the wave. Even with that high resolution of DNS 1 the largest differences between simulation and experiment occur in this region. In the simulation the u-velocity averaged over planes $\eta = const.$ has a maximum of $1.245\,U$ at a height $\eta/H = 0.639$, so the maximum is shifted by more than $2\delta/H$ in upward direction. The position of the experimental maximum is unknown. The separated region, bounded by the streamline $\Psi = 0$, extends from $x/\lambda = 0.15$ to $x/\lambda = 0.59$ in the DNS compared to

$x/\lambda = 0.3$ and $x/\lambda = 0.5$ in the experiment. One has to remind the coarse experimental streamwise resolution of $\Delta x/\lambda \leq 0.1$.

Because the vertical velocity component (Figure 4 b) is approximately coupled with the streamwise velocity component the greatest differences between DNS and experiment occur at the same positions, namely at the upslope side of the wave.

The component $-\overline{u'w'}$ of the Reynolds stress tensor is shown in Figure 4 c). At the upslope side $-\overline{u'w'}$ becomes negative near the wall. This is an artefact of calculating the Reynolds stress in Cartesian coordinates. Here the measurements are in good agreement with the numerical results. At the downslope surface $-\overline{u'w'}$ should be positive inside as well as outside the separated region, but the experiment has negative values at the first measurement points from the wall.

The rms-value of u (Figure 4 d) in the DNS develops a relative maximum near the surface at $x/\lambda \approx 0.8$ and reaches an absolute maximum over the next trough. If one defines a shear layer through an intensity maximum of the turbulent velocity fluctuations [5], two shear layers can be discerned for positions $0.8 \leq x/\lambda \leq 1.3$. The agreement with the experiment is very good. The intensity of the v-velocity (Figure 4 e) reaches a maximum of $\sqrt{\overline{v'^2}}/U_{\mathrm{ref}} = 0.2$ at a streamwise position $x/\lambda = 0.69$ which is about $0.1\,x/\lambda$ behind the reattachment point. In this region the v-component gives a large contribution to the turbulence energy near the surface. The rms-value of the w-velocity (Figure 4 f) has its absolute maximum near $x/\lambda = 0.55$. The agreement with the experiment is very good at the upslope side of the wave whereas at the downslope side the experiment shows higher intensities near the bottom at $0.1 \leq x/\lambda \leq 0.4$.

In general the experimental values seem to deviate systematically from the expected and computed results near the center of the channel. Because the spreading near the surfaces is very high we assume that the measurements suffer from some disturbing influences from the wall. Although the number of experimental samples is three times the number of DNS samples the measurements show individual data points far outside the expected statistical spread.

The pressure field is responsible for the form drag of the wavy wall. The figure assumed from a potential flow is disturbed by the separated region and the stagnation point at the location of reattachment (Figure 5). In the simulation the isolines $p/(\rho U^2) = 0.0$ and 0.1 show the effect of the recirculation, decreasing the pressure gradient in x-direction along $\Psi = 0$. In the experimental pressure field, which was obtained indirectly by calculating it from the measured velocity field using a reference pressure measured near the channel center, such effect is not seen. The location of the absolute maximum of the surface pressure is located at $x/\lambda = 0.65$ for the DNS which is $0.05\,x/\lambda$ behind the reattachment point. In the experiment this shift is $0.1\,x/\lambda$. The values of the surface pressure maxima are $2(p-p_{\mathrm{ref}})/(\rho\,U_{\mathrm{ref}}^2) = 0.38$ and 0.81 for the experiment and the simulation, respectively. Because the numerical results agree very well with values from similar experiments [5, 10] we assume that the experimental results from Hudson are too high by a factor of 2. The maximum of pressure intensities (not shown) coincides with the surface pressure maximum. From this comparison the indirect experimental determination of the pressure field from the measured velocity field seems not to be able to substitute direct pressure measurements.

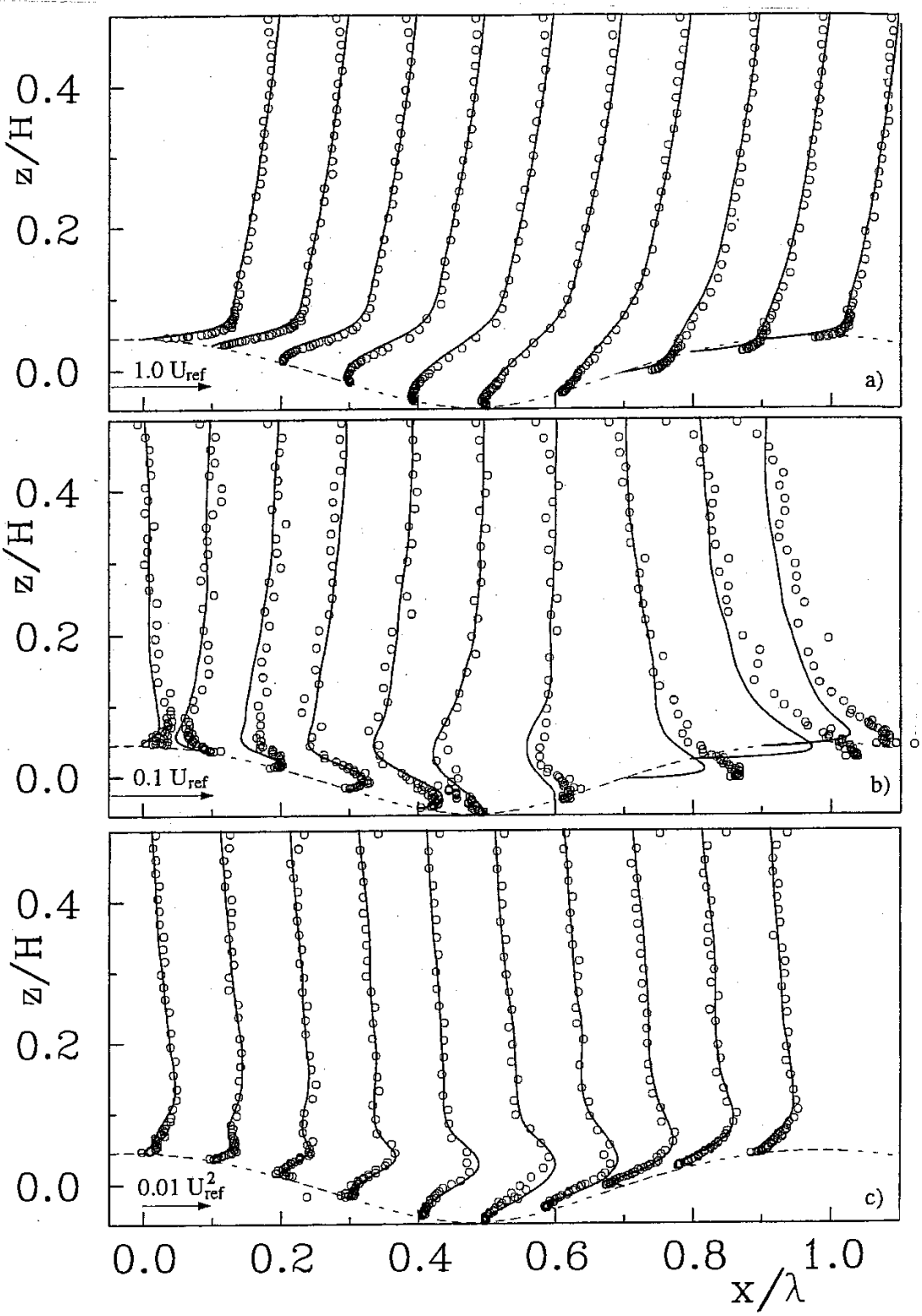

Figure 4: Comparison of DNS 1 and experiment by means of vertical flow profiles at positions $x/\lambda = 0.0, 0.1 \ldots, 0.9$, referenced with $U_{\mathrm{ref}} = 0.912\,\dot{U}$ (The respective origin is on the bottom ordinate). —— ytp-averaged results of DNS 1, ∘ LDA measurements [13], a) $\overline{u}/U_{\mathrm{ref}}$ b) $\overline{w}/U_{\mathrm{ref}}$ c) $-\overline{u'w'}/U_{\mathrm{ref}}^2$ d) $\sqrt{\overline{u'^2}}/U_{\mathrm{ref}}$ e) $\sqrt{\overline{v'^2}}/U_{\mathrm{ref}}$ f) $\sqrt{\overline{w'^2}}/U_{\mathrm{ref}}$.

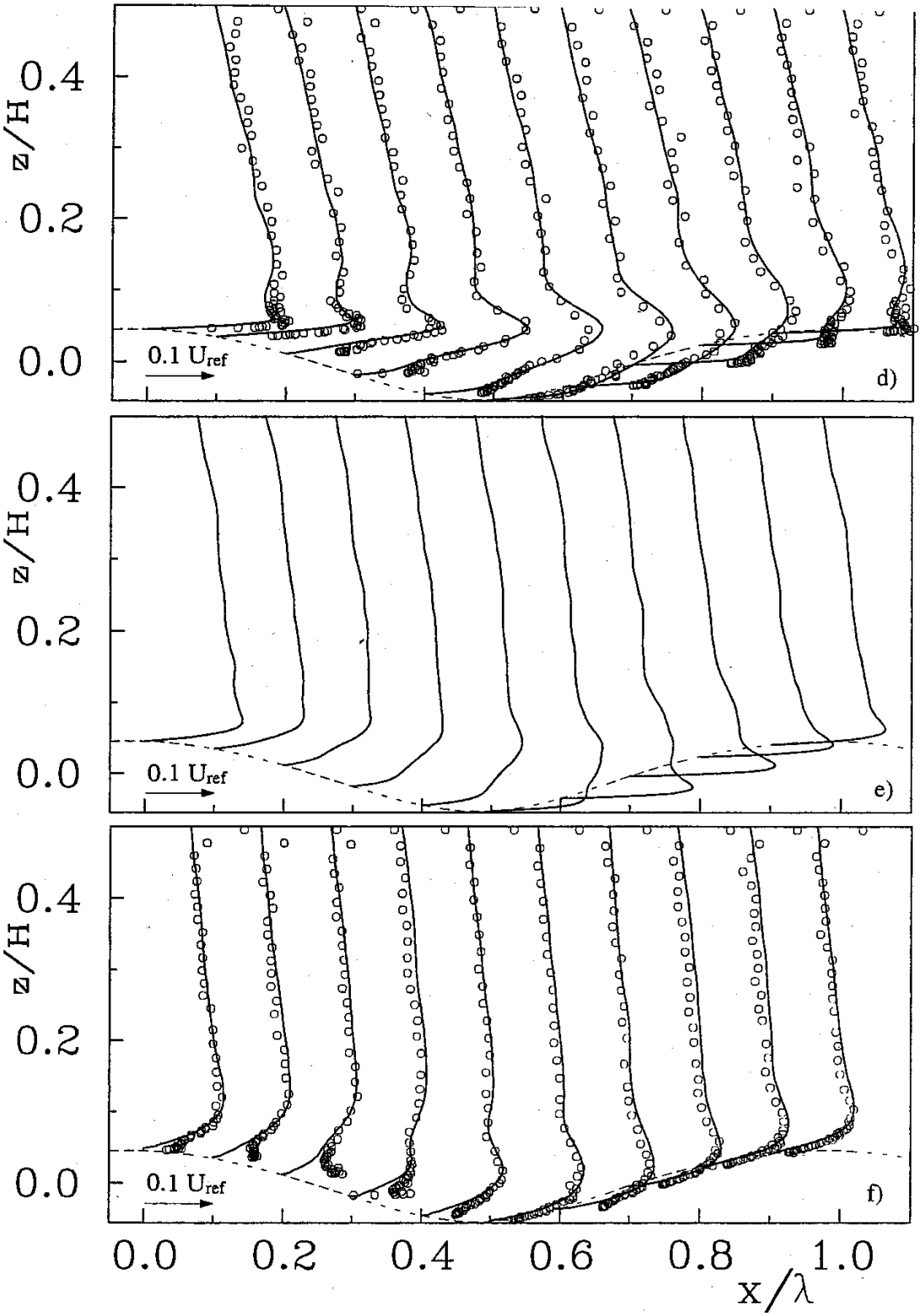

Figure 4: Continuation.

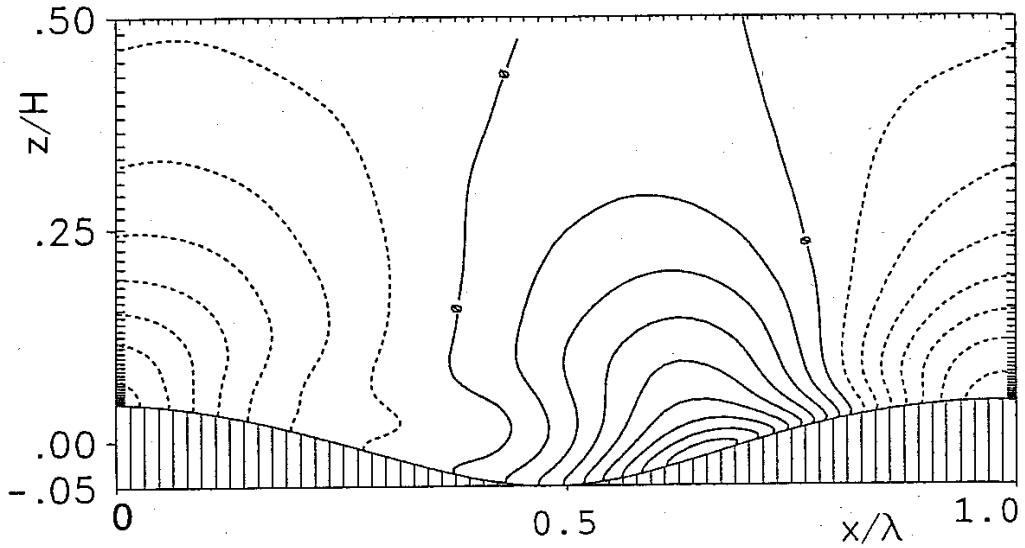

b)

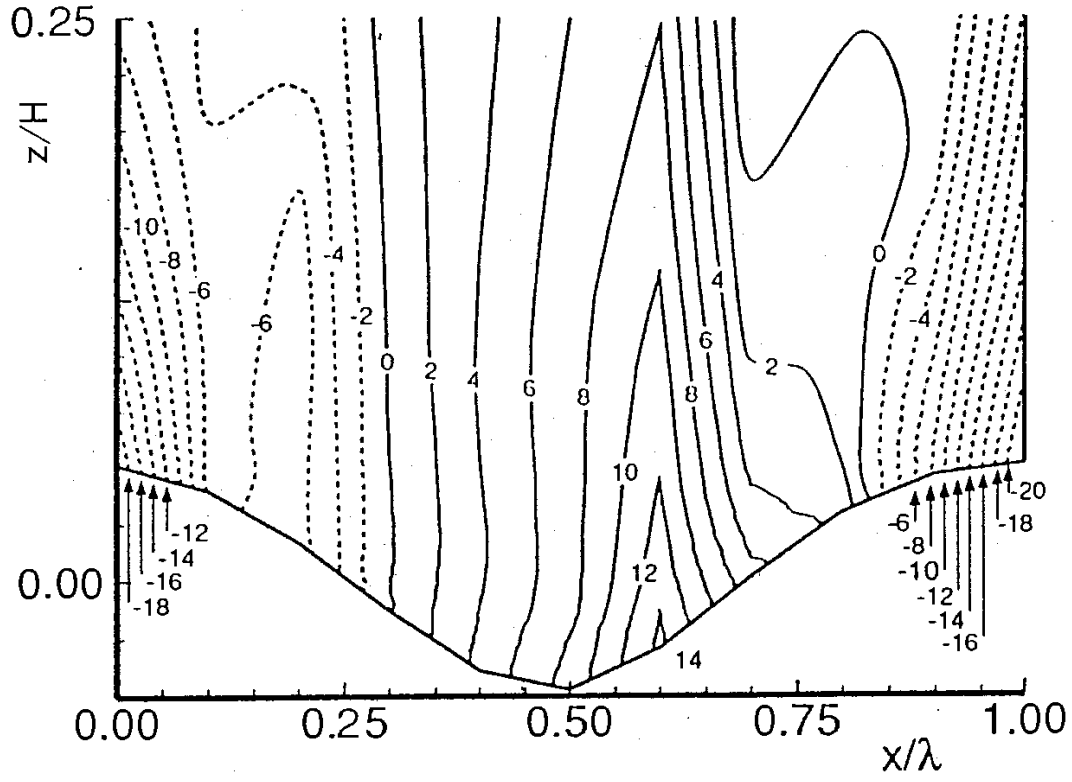

Figure 5: Mean pressure field (— positive values, - - - negative values). a) ytp-averaged pressure field $\overline{p}/(\rho U^2)$ of DNS 1 (mean pressure gradient P_x subtracted, increment 0.01), b) time averaged pressure field $\overline{p}/(\rho u_{\tau,\mathrm{wa}}^2)$ deduced from velocity measurements of the experiment [13].

Conclusion

In this study, direct numerical simulations of turbulent flow over a wavy boundary have been carried out and compared to measurements by Hudson [13]. Our method is able to predict the main features of separated flow and the flow structure can be described. In particular we find that a recirculation zone develops. At $Re = 6760$ this recirculation zone could be simulated with a rather coarse grid but only if a variable vertical grid spacing is used with finer resolution of the order of ν/u_τ near the walls. Mainly because of the additional pressure drag, the effective friction velocity is about 50% larger at the wavy lower surface than at the flat upper surface. The computed local mean velocity profiles and mean turbulence profiles agree rather well with the measurements. The size of the separation zone in the simulation is larger than in the experiment, which yields a smaller pressure drag. We have shown that the influence of the Reynolds number at such low turbulence levels is rather small whereas the shape of the bottom surface is of great importance.

From this comparison between simulation and experiment we conclude that our method is at least as precise as laboratory measurements.

Acknowledgement

The authors thank the Deutsche Forschungsgemeinschaft (DFG) for supporting this study in its Priority Research Program 'Strömungssimulation mit Hochleistungsrechnern'. We also thank Dr. J. D. Hudson and Professor T. J. Hanratty for providing the experimental data and for recalculating some results.

References

[1] G. P. Almeida, D. F. G. Durão, and M. V. Heitor. Wake flows behind two-dimensional model hills. *Experimental Thermal and Fluid Science*, 7:87–101, 1993.

[2] A. Andrén, A. R. Brown, J. Graf, P. J. Mason, C.-H. Moeng, F. T. M. Nieuwstadt, and U. Schumann. Large-eddy simulation of a neutrally stratified boundary layer: A comparison of four computer codes. *Q. J. R. Meteorol. Soc.*, 120:1457–1484, 1994.

[3] T. B. Benjamin. Shearing flow over a wavy boundary. *J. Fluid Mech.*, 6:161–205, 1959.

[4] M. Breuer and W. Rodi. Large-eddy simulation of complex flows of practical interest. In this publication.

[5] J. J. Buckles, T. J. Hanratty, and R. J. Adrian. Turbulent flow over large-amplitude wavy surfaces. *J. Fluid Mech.*, 140:27–44, 1984.

[6] M. Dianat and I. P. Castro. Turbulence in a separated boundary layer. *J. Fluid Mech.*, 226:91–123, 1991.

[7] A. Dörnbrack, T. Gerz, and U. Schumann. Turbulent breaking and overturning gravity waves below a critical level. *Appl. Sci. Res.*, 54:163–176, 1995.

[8] A. Dörnbrack and U. Schumann. Numerical simulation of turbulent convective flow over wavy terrain. *Boundary-Layer Meteorol.*, 65:323–355, 1993.

[9] J. G. M. Eggels, F. Unger, M. H. Weiss, J. Westerweel, R. J. Adrian, R. Friedrich, and F. T. M. Nieuwstadt. Fully developed turbulent pipe flow: a comparison between direct numerical simulation and experiment. *J. Fluid Mech.*, 268:175–209, 1994.

[10] W. Gong, P. A. Taylor, and A. Dörnbrack. Turbulent boundary-layer flow over fixed, aerodynamically rough, 2-d sinusoidal waves. *J. Fluid Mech.*, 1996. in press.

[11] C. Härtel and L. Kleiser. Large-eddy simulation of near-wall turbulence. In this publication.

[12] M. Hino and T. Okumura. Coherent structure of turbulent flow over wavy walls. In *Proc. 9th Turbulent Shear Flow Symp. Kyoto, Aug. 16-18*, pages 14.3.1–4, 1993.

[13] J. D. Hudson. *The effect of a wavy boundary on turbulent flow.* PhD thesis, Dept. Chemical Engineering, University of Illinois, Urbana, 1993.

[14] T. Kajishima, Y. Miyake, and T. Ohta. Direct numerical simulation of turbulent flow in a wavy channel. In *Proc. of The International Symp. on Mathematical Modelling of Turbulent Flows. Tokyo, Dec. 18-20*, pages 176–180, 1995.

[15] J. Kim, P. Moin, and R. Moser. Turbulence statistics in fully developed channel flow at low reynolds number. *J. Fluid Mech.*, 177:133–166, 1987.

[16] K. Krettenauer and U. Schumann. Numerical simulation of turbulent convection over wavy terrain. *J. Fluid Mech.*, 237:261–299, 1992.

[17] J. D. Kuzan, T. J. Hanratty, and R. J. Adrian. Turbulent flows with incipient separation over solid waves. *Exper. in Fluids*, 7:88–98, 1989.

[18] H. Lamb. *Hydrodynamics.* Dover, New York, 1945.

[19] C. Maaß, A. Dörnbrack, and U. Schumann. Grobstruktursimulationen turbulenter Strömungen über welligem Untergrund. Deutsche Meteorologen-Tagung, 16.-20.3.1992, Berlin. In *Ann. Meteorol.*, volume 27, pages 306–307, 1992.

[20] C. Maaß and U. Schumann. Numerical simulation of turbulent flow over a wavy boundary. In P. R. Voke, L. Kleiser, and J.-P. Chollet, editors, *Direct and large-eddy simulation I: selected papers from the First ERCOFTAC Workshop on Direct and Large-Eddy Simulation*, pages 287–297. Kluwer Academic Press, Dordrecht, 1994.

[21] H. Motzfeld. Die turbulente Strömung an welligen Wänden. *Z. angew. Math. Mech.*, 17:193–212, 1937.

[22] W. Rodi, editor. *ERCOFTAC Workshop on Data Bases and Testing of Calculation Methods for Turbulent Flows*, Karlsruhe, April 3-7 1995.

[23] U. Schumann. Large-eddy simulation of turbulent convection over flat and wavy terrain. In B. Galperin and S. A. Orszag, editors, *Large-Eddy Simulation of Complex Engineering and Geophysical Flows*, pages 399–421. Cambridge Univ. Press, 1993.

[24] U. Schumann. Stochastic backscatter of turbulence energy and scalar variances by random subgrid-scale fluxes. *Proc. Roy. Soc. London A*, 451:293–318 and 811, 1995.

[25] U. Schumann and M. Strietzel. Parallel solution of tridiagonal systems for the Poisson equation. *J. Sci. Comput.*, 10:181–190, 1995.

[26] C. B. Thorsness, P. E. Morrisroe, and T. J. Hanratty. A comparison of linear theory with measurements of the variation of shear stress along a solid wave. *Chem. Eng. Sci.*, 33:579–592, 1978.

[27] F. Unger. *Numerische Simulation turbulenter Rohrströmungen.* PhD thesis, Technische Universität, München, 1994.

[28] N. Wood and P. Mason. The pressure force induced by neutral, turbulent flow over hills. *Q. J. R. Meteorol. Soc.*, 119:1233–1267, 1993.

[29] D. P. Zilker, G. W. Cook, and T. J. Hanratty. Influence of the amplitude of a solid wavy wall on a turbulent flow. Part 1. Non-separated flows. *J. Fluid Mech.*, 82:29–51, 1977.

[30] D. P. Zilker and T. J. Hanratty. Influence of the amplitude of a solid wavy wall on a turbulent flow. Part 2. Separated flows. *J. Fluid Mech.*, 90:257–271, 1979.